



# Halogenated cyanine dyes for synergistic photodynamic and photothermal therapy

Hao Liu, Juanjuan Yin, Enyun Xing, Yingying Du, Yu Su, Yaqing Feng, Shuxian Meng<sup>\*</sup>

School of Chemical Engineering and Technology, Tianjin University, Yaguan Road 135, Tianjin, 300050, PR China

## ARTICLE INFO

### Keywords:

Cyanine dye  
Photodynamic therapy  
Photothermal therapy  
Phototheranostic  
Heavy atom effect

## ABSTRACT

Cyanine dyes are widely used in the field of tumor phototherapy due to their excellent photophysical properties. To explore the heavy atoms effects on the photothermal and photodynamic performance of phototherapeutic agents, chlorine, bromine, and iodine were introduced to synthesize a series of cyanine dyes (IR6, IR7, and IR8). We have found that all halogenated cyanine dyes exhibited high excitation wavelength (around 800 nm) and low dark toxicity. Among them, IR8 behaved the best singlet oxygen production ability in the three dyes. For photothermal performance, IR8 exhibited the best photothermal conversion rate (46.6%), photothermal stability, and excellent therapy efficiency (half-maximal inhibitory concentration,  $IC_{50} = 16.2 \mu\text{g/mL}$ ). IR7 behaved a greater enhancement of the photothermal conversion rate (43.4%) than IR6 (42.3%). In conclusion, the heavy atoms effects on the photothermal and photodynamic properties of cyanine dyes are positively correlated with the increase of the atomic number of the halogen atom, and the iodine atom may be the most worthy of consideration in the all halogen atoms.

## 1. Introduction

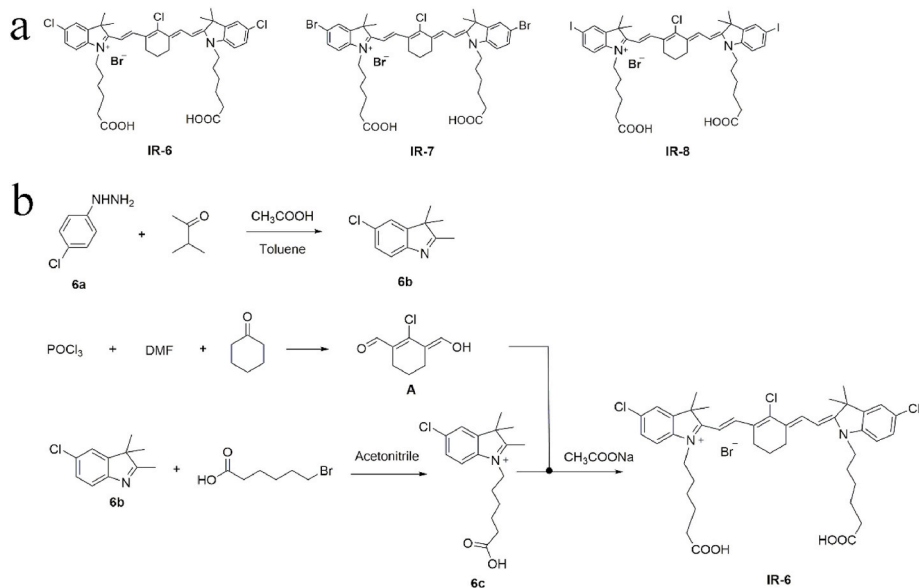
Cancer is the leading cause of consistently high morbidity and mortality worldwide [1]. Traditional cancer treatments include chemotherapy, radiation therapy, and surgical treatment. However, these treatments always make patients suffer from serious side effects and drug resistance [2,3]. As one of the new treatments for cancer, phototherapy has attracted widespread attention from researchers due to its excellent properties such as non-invasiveness, high tumor suppression, and high safety in tumor treatment [4]. Phototherapy mainly includes photothermal therapy (PTT) and photodynamic therapy (PDT) [5]. Among them, PTT is a method that uses photothermal agents (PTAs) to convert light energy into thermal energy to generate high temperature and kill cancer cells under laser irradiation [6]. However, the photothermal effect will be affected by the uneven distribution of PTAs in tumors, leading to inefficient treatment [7]. Besides, the heat resistance caused by the overexpression of heat shock proteins in some cancers also makes the treatment less effective [8]. For PDT, reactive oxygen species (ROS), especially singlet oxygen ( $^1\text{O}_2$ ), produced by photosensitizers (PSs) under laser irradiation can induce cell apoptosis [9,10]. However, the hypoxic microenvironment at the tumor site limits the production of reactive oxygen species and therefore prevents PS

from exerting effective photodynamic effects [11]. How to overcome the defects of PTT and PDT and achieve better tumor treatment effects, has been an important target for researchers. And various new strategies combining different tumor treatment methods have been developed. For example, synergistic therapy, which combines PDT and PTT, can use the photothermal conversion capacity of phototherapy agents to generate heat to kill most tumor cells avoiding being influenced by the hypoxic environment. Besides, the PSs can produce more ROS to kill tumor cells with higher temperature achieving the effect of “1 + 1 > 2” [12,13]. Therefore, it is a particularly important method to develop phototherapy agents that have excellent photothermal and photodynamic therapeutic effects.

Indocyanine green (ICG), is the only Food and Drug Administration (FDA) approved NIR agent [14]. It has also been explored as a potential photosensitizer, but the disadvantages of photobleaching and low singlet oxygen quantum yield have limited its practical application [15]. Therefore, a new kind of indocyanine green derivatives (Cypate [16], IR780 [17], IR808 [18], IR825 [19], etc.) have been synthesized as photosensitizers and photothermal agents. Among them, a heptamethine, IR-808 [20], was developed not only with NIR imaging properties and good biocompatibility but also with photosensitizing activities [18, 21]. However, the therapeutic efficacy of IR-808, as well as many other

<sup>\*</sup> Corresponding author. School of Chemical Engineering and Technology, Tianjin University, Tianjin, 300050, PR China.

E-mail address: [msxmail@tju.edu.cn](mailto:msxmail@tju.edu.cn) (S. Meng).



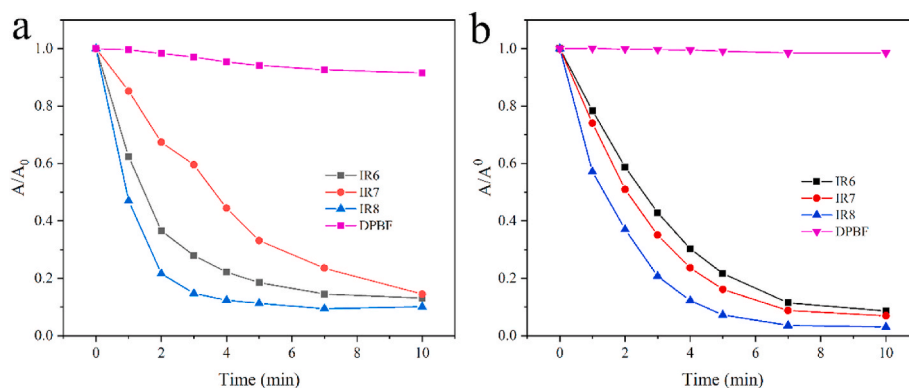


Fig. 3. The absorbance of DPBF with IR6, IR7, and IR8 in (a) water and (b) DMF under laser in 10 min.

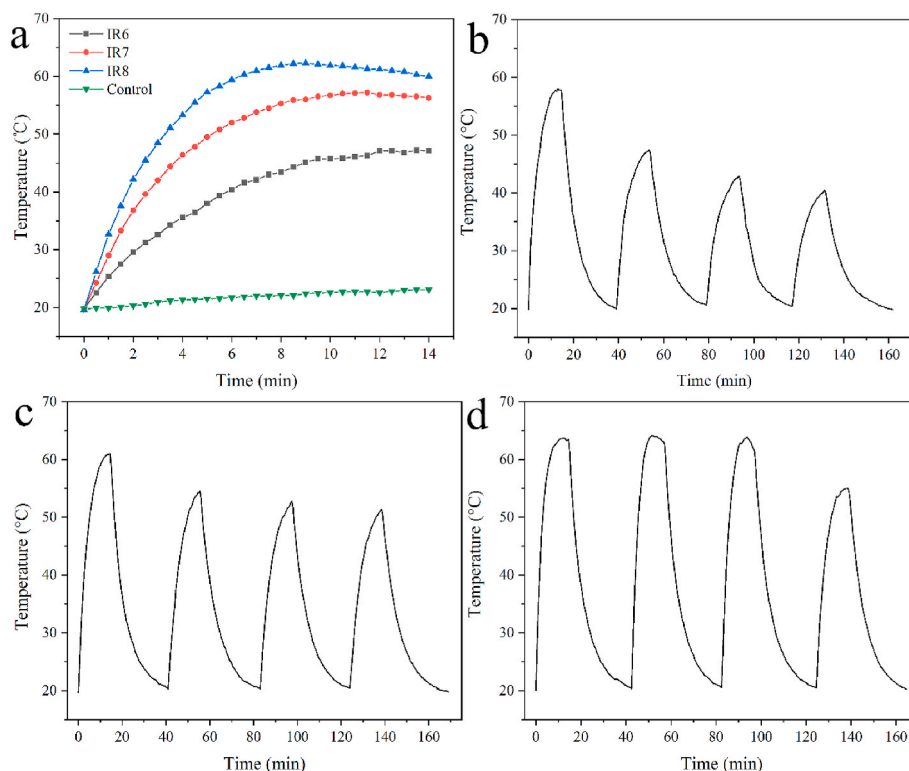


Fig. 4. (a) Temperature elevation for IR6, IR7, and IR8 (40  $\mu\text{g/mL}$ ) in water (10% DMF) under the irradiation of 808 nm laser at 1.0  $\text{W/cm}^2$ . Photothermal stability experiments with alternate heating and cooling cycles of (b) IR6, (c) IR7, and (d) IR8 using an 808 nm laser at 1.0  $\text{W/cm}^2$ .

with the absorption/emission wavelength, photothermal conversion efficiency, and photothermal stability was positively correlated with the increase of the atomic number of the halogen atom. However, the increase of the atomic number of halogen atom did not show a correlation with the increase in the photodynamic effect. Moreover, IR8 exhibited various advantages of an ideal PS with high photothermal conversion rate, enhanced ROS production ability, low dark toxicity, and photocytotoxicity.

## 2. Experimental section

### 2.1. Materials and instruments

4-chlorophenylhydrazine hydrochloride, 4-bromophenylhydrazine hydrochloride, 4-iodophenylhydrazine hydrochloride, and 6-bromohexanoic acid were obtained from Heowns-opde Co., Ltd. (Tianjin, China). 3-methyl-2-butanone, cyclohexanone, and sodium acetate were

purchased from Aladdin (Shanghai, China). All the raw chemicals were purchased from commercial sources and used without further purification. 1,3-diphenylisobenzofuran (DPBF) and 3-(4,5-dimethylthiazol-2-yl)-2,5-diphenyltetrazolium bromide (MTT) were bought from Beyotime Biotechnology. Dulbecco's modified Eagle medium (DMEM), penicillin/streptomycin fetal bovine serum (FBS), phosphate buffered saline (PBS) were obtained from Baibei Biotechnology Co., Ltd. (Suzhou, China).

$^1\text{H}$  NMR and  $^{13}\text{C}$  NMR spectra were recorded on a Bruker Avance 400 MHz. High-resolution mass spectra (HRMS) were recorded on a Shimadzu ESI-MS instrument. UV-Vis absorption spectra were recorded on a Shimadzu UV-1800 spectrophotometer. Fluorescence spectra were recorded on an Agilent Cary Eclipse fluorescence spectrophotometer. The temperature changes of samples were recorded by an infrared imager (FLIR E6). All measurements were carried out at room temperature in the ambient atmosphere.

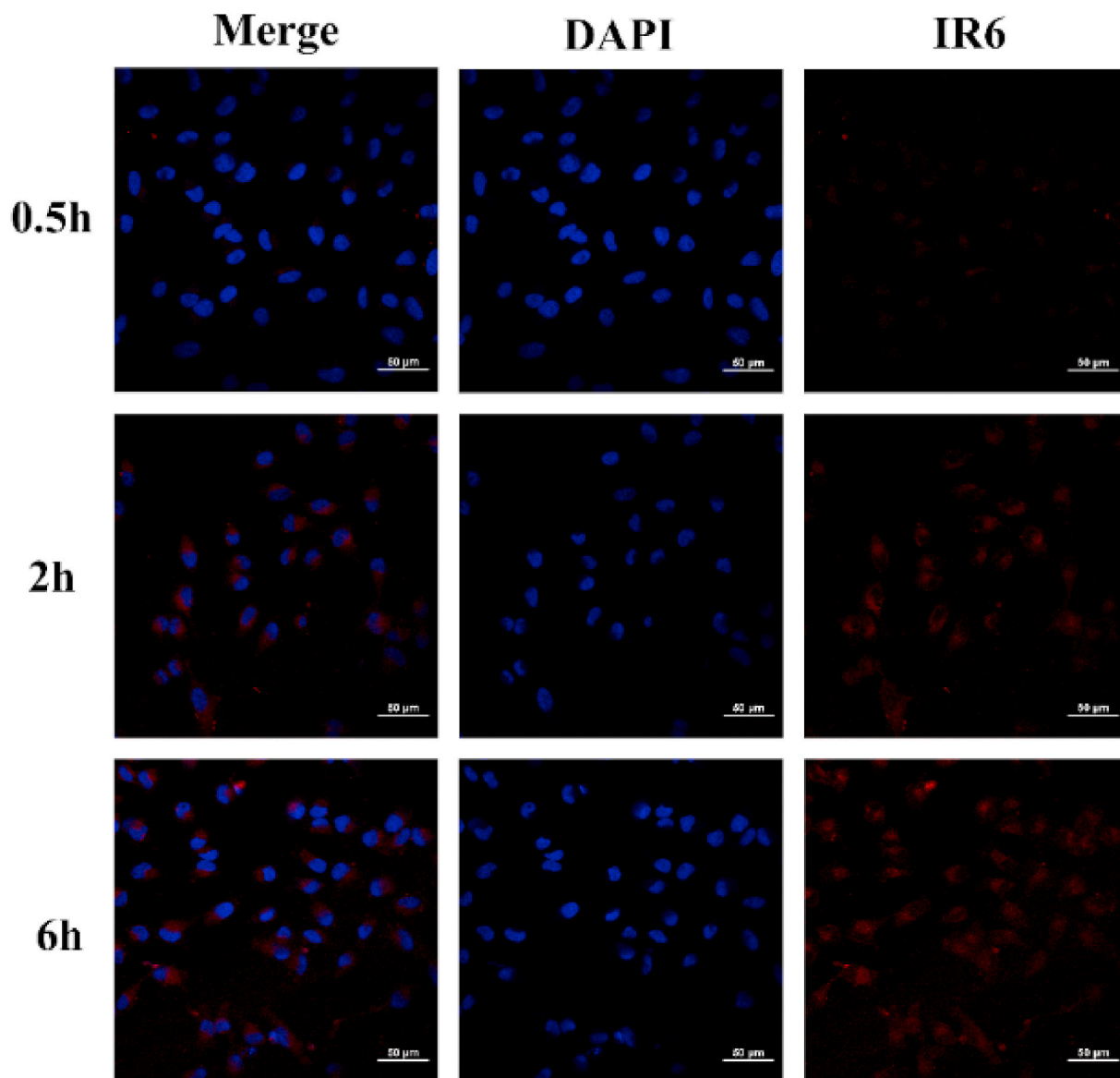


Fig. 5. The CLSM images of HeLa cells incubated with IR6 (40 µg/mL).

## 2.2. Preparation of IR6

We prepared three halogenated derivatives of cyanine, whose 5-position of indole ring was substituted by chlorine (IR6), bromine (IR7), and iodine (IR8), respectively. In the case of IR6, chlorophenylhydrazine hydrochloride was refluxed with 3-methyl-2-butanone to produce the indole 6b, which with 6 bromohexanoic acid resulted in the formation of derivative 6c by *N*-alkylation reaction. Meanwhile, 2-chloro-1-formyl-3-hydroxymethylcyclohexene (A) was prepared by cyclohexanone, phosphoryl chloride, and dimethylformamide using Vilsmeier–Haack reaction. Finally, the compound 6c and A were used to produce the target compound IR6 by a condensation reaction. Besides, compound IR7 and IR8 were prepared according to the reported method [25,26]. The synthetic route is shown in Fig. 1b.

### 2.2.1. Synthesis of 2-chloro-1-formyl-3-hydroxymethylcyclohexene (A)

In a 250 mL three-necked flask, DMF (24 mL) was added to and cooled in an ice bath at 0 °C. Then, POCl<sub>3</sub> (4.6 g, 30 mmol) was added and the mixture was stirred for 30 min. Cyclohexanone (2.5 g, 25 mmol) was added and the solution was refluxed at 80 °C for 4 h. The red mixture was slowly poured into a 100 mL beaker with 50 g ice water

mixture and stirred for 1 h at room temperature. The yellow solid was precipitated, then filtered and washed with water. The purified A was obtained by recrystallization from dichloromethane. (3.69 g, 85.6%). <sup>1</sup>H NMR (400 MHz, DMSO-*d*<sub>6</sub>) δ 2.34 (t, *J* = 6.2 Hz, 4H), 1.57 (q, *J* = 6.2 Hz, 2H).

### 2.2.2. Synthesis of 5-chloro-2,3,3-trimethyl-3H-indole (6b)

4-chlorophenylhydrazine hydrochloride (6a) (4 g, 22.3 mmol) and 3-methyl-2-butanone (2.3 mL, 26.7 mmol) were added to a 100 mL double-necked flask. Afterwards, ethanol (25 mL) and sulfuric acid (3 mL, 95%) was added. The mixture was refluxed at 85 °C for 5 h and was evaporated in vacuum. The brown solution was washed three times with saturated NaHCO<sub>3</sub> solution and water. The organic layer was dried over Na<sub>2</sub>SO<sub>4</sub> and evaporated. A thick red-brown liquid was the purified compound 6b (3.59 g, 83.02%). <sup>1</sup>H NMR (400 MHz, CDCl<sub>3</sub>) δ 7.40 (s, 1H), 7.25 (d, *J* = 2.2 Hz, 1H), 7.22 (s, 1H), 2.24 (s, 3H), 1.28 (s, 6H).

### 2.2.3. Synthesis of 1-(5-carboxypentyl)-5-chloro-2,3,3-trimethyl-3H-indolium (6c)

In 100 mL double-necked flask, 5-chloro-2,3,3-trimethyl-3H-indole (6b) (3.13 g, 16.2 mmol) and 6-bromohexanoic acid (3 mL, 21.7

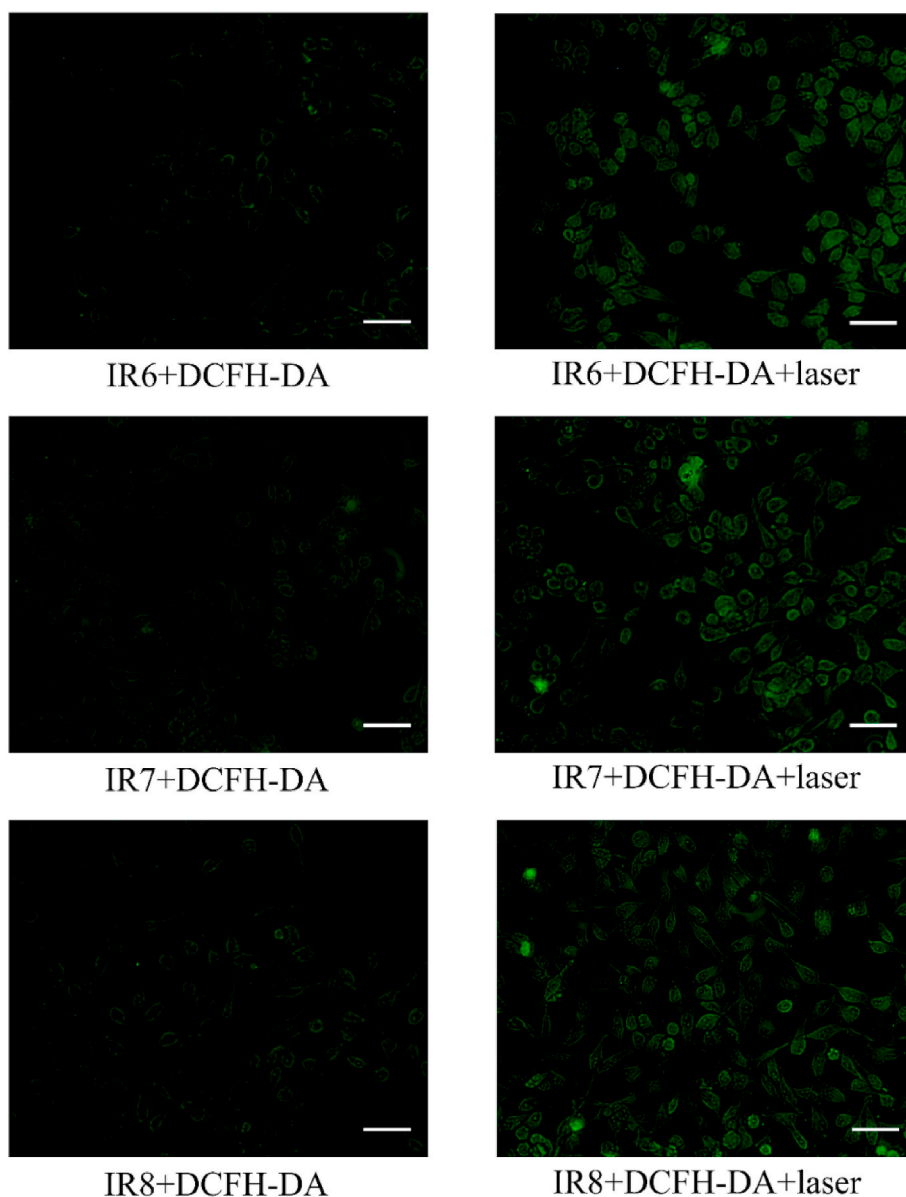


Fig. 6. Fluorescence microscope images of HeLa cells incubated with IR6, IR7, and IR8 with laser irradiation (right) or without (left). The scale bar is 50  $\mu\text{m}$ .

mmol) were dissolved in 30 mL of acetonitrile. The mixture was refluxed at 85  $^{\circ}\text{C}$  for 60 h under shading. Then, the mixture was cooled to room temperature and evaporated in vacuum. The crude material was purified by normal phase flash chromatography with  $\text{CH}_2\text{Cl}_2$ : MeOH (15:1 v/v) for 6c to obtain a purple liquid (3.67 g, 73.4%).  $^1\text{H}$  NMR (400 MHz,  $\text{DMSO}-d_6$ )  $\delta$  8.07 (d,  $J = 2.0$  Hz, 1H), 8.03 (d,  $J = 8.6$  Hz, 1H), 7.72 (dd,  $J = 8.6, 2.1$  Hz, 1H), 4.45 (t,  $J = 7.8$  Hz, 3H), 2.85 (s, 3H), 2.23 (t,  $J = 7.2$  Hz, 3H), 1.88–1.77 (m, 3H), 1.55 (s, 8H), 1.47–1.37 (m, 3H).  $^{13}\text{C}$  NMR (500 MHz,  $\text{DMSO}-d_6$ )  $\delta$  197.86, 175.07, 144.64, 140.63, 135.00, 129.69, 124.76, 55.13, 48.44, 34.06, 27.55, 26.04, 24.71, 22.50. Electro-Spray ionization tandem mass spectrometry (ESI-MS)  $m/z$  found:  $[\text{M}+\text{H}]^+$  308.1414; molecular formula  $\text{C}_{17}\text{H}_{23}\text{ClNO}_2^+$  requires  $[\text{M}+\text{H}]^+$  308.1412.

#### 2.2.4. Synthesis of 1-(5-carboxypentyl)-2-((E)-2-((E)-3-(2-((E)-1-(5-carboxypentyl)-5-chloro-3,3dimethylindolin-2-ylidene)ethylidene)-2-chlorocyclohex-1-en-1-yl)vinyl)-5-chloro-3,3dimethyl-3H-indol-1-ium (IR6)

In 100 mL double-necked flask, a mixture of 6c (281.2 mg, 0.36 mmol), A (31.1 mg, 0.2 mmol) and anhydrous sodium acetate (30.4 mg,

0.37 mmol) were dissolved in acetic anhydride (16 mL). Then, the mixture was heated at 70  $^{\circ}\text{C}$  and stirred for 2 h under an  $\text{N}_2$  atmosphere to obtain the cyanine. Afterwards, the green solution was cooled to room temperature, and acetic anhydride was removed by rotavap. The mixture was purified by normal phase flash chromatography with  $\text{CH}_2\text{Cl}_2$ : MeOH (20:1 v/v) to obtain the purified IR6 (160 mg, 53.1%).  $^1\text{H}$  NMR (400 MHz, MeOD)  $\delta$  8.41 (d,  $J = 14.0$  Hz, 2H), 7.58 (d,  $J = 2.0$  Hz, 2H), 7.42 (dd,  $J = 8.5, 2.0$  Hz, 2H), 7.32 (d,  $J = 8.6$  Hz, 2H), 6.29 (d,  $J = 14.1$  Hz, 2H), 4.16 (t,  $J = 7.4$  Hz, 4H), 2.72 (t,  $J = 6.2$  Hz, 4H), 2.28 (t,  $J = 7.3$  Hz, 4H), 1.98–1.91 (m, 2H), 1.89–1.79 (m, 4H), 1.72 (s, 12H), 1.70–1.65 (m, 4H), 1.48 (dd,  $J = 10.4, 4.8$  Hz, 4H).  $^{13}\text{C}$  NMR (400 MHz,  $\text{CD}_3\text{OD}$ )  $\delta$  172.58, 150.11, 144.20, 143.08, 141.02, 130.64, 127.36, 122.74, 112.12, 101.37, 49.35, 43.92, 34.12, 26.79, 26.66, 26.04, 24.58. Electro-Spray ionization tandem mass spectrometry (ESI-MS)  $m/z$  found:  $[\text{M}+\text{H}]^+$  753.2814; molecular formula  $\text{C}_{42}\text{H}_{50}\text{Cl}_3\text{N}_2\text{O}_4^+$  requires  $[\text{M}+\text{H}]^+$  753.2801.

#### 2.3. UV-vis and fluorescence spectroscopy

IR6, IR7, and IR8 solutions (5  $\mu\text{g}/\text{mL}$ ) were prepared by dissolving

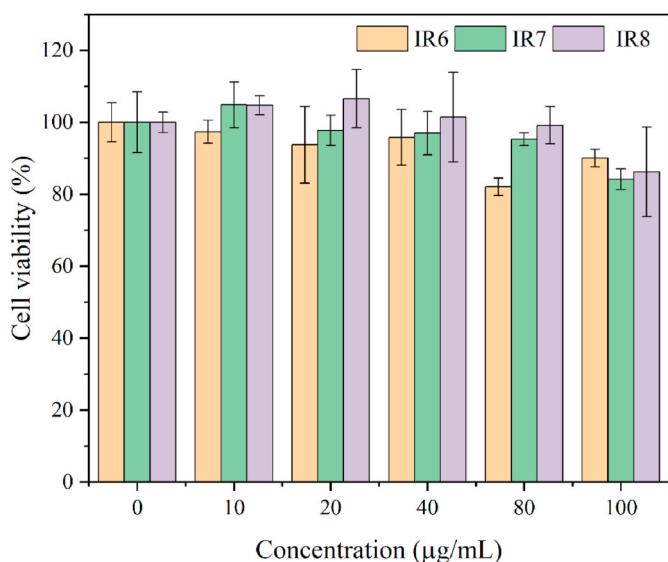


Fig. 7. Cell viability of HeLa cells incubated with IR6, IR7, and IR8 for 24 h.

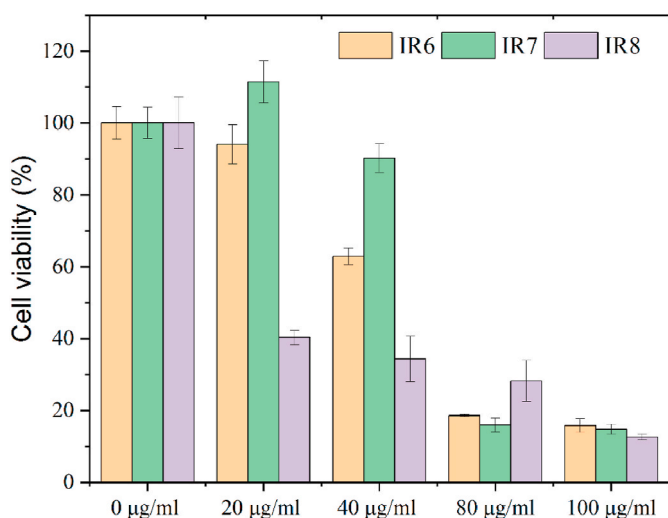


Fig. 8. Cell viability of HeLa cells incubated with IR6, IR7, and IR8 with laser irradiation.

the appropriate amount of each dye in methanol, *N,N*-dimethylformamide (DMF), and water. Absorption spectra were measured by a UV–Vis spectrophotometer (UV-1800, Shimadzu, Japan). Fluorescence spectra were recorded on an Agilent Cary Eclipse fluorescence spectrophotometer.

#### 2.4. Singlet oxygen detection in vitro

To evaluate the generation of singlet oxygen from samples, 1,3-diphenylisobenzofuran (DPBF, 1 mg/mL) was used as a singlet oxygen catcher. The mixture solutions of DPBF with IR6, IR7, and IR8 (10 µg/mL) in water and DMF were irradiated using 808 nm laser (0.4 W/cm<sup>2</sup>). The degradation of DPBF was determined by a UV–Vis spectrophotometer at different times (0, 1, 2, 3, 4, 5, 7, 10 min).

#### 2.5. Photothermal effect

The photothermal properties of IR6, IR7, and IR8 were determined using a reported method [27]. Briefly, the solutions of IR6, IR7, and IR8 at different concentrations (0, 10, 20, 40, and 80 µg/mL) were placed in

1 mL centrifuge tubes and irradiated by a NIR laser (808 nm, 1.0 W/cm<sup>2</sup>) for 14 min at room temperature. The laser was then switched off, and the solutions were cooled naturally. The temperatures of the solutions during laser irradiation and cooling process were both recorded in real-time using a FLIR E6 thermal imager.

The photothermal conversion efficiency ( $\eta$ ) of dyes was evaluated according to a reported method [28,29]. The  $\eta$  of dyes was calculated using the following equation:

$$\eta = \frac{hA(\Delta T_{max,mix} - \Delta T_{max,H_2O})}{I(1 - 10^{-A_{808}})}$$

$$\tau_s = \frac{m_p C_p}{hA}$$

$h$  is the heat transfer coefficient,  $A$  is the surface area of the container, and the value of  $hA$  is calculated.  $\Delta T_{max,mix}$  and  $\Delta T_{max,H_2O}$  are the temperature changes of the dispersion and solvent at the maximum steady-state temperature, respectively,  $I$  is the laser power and  $A_{808}$  is the absorbance of dyes at 808 nm  $m_D$  and  $C_D$  are the mass and heat capacity (4.2 kJ/kg) of the deionized water used as the solvent.

#### 2.6. Photothermal stability

The solutions of IR6, IR7, and IR8 (80 µg/mL) were placed in 1 mL centrifuge tubes and irradiated by a NIR laser (808 nm, 1.0 W/cm<sup>2</sup>) for 14 min. The laser was then switched off, and the solution was cooled to room temperature naturally. This operation was repeated four times.

#### 2.7. Cellular uptake test

To assess the cellular uptake of IR6, IR7, and IR8, HeLa cells ( $1 \times 10^5$  cells/mL) were seeded into 48-well plates and cultured for 24 h. After that, the fresh medium containing sample concentrations of dyes (IR6, IR7, and IR8, 40 µg/mL) were substituted for the original culture medium and incubated for different time (0.5 h, 2 h, and 6 h). Then the cells were washed with PBS for 3 times and treated with a 4% paraformaldehyde solution (0.5 mL) for 20 min. Subsequently, the cells were stained with 4,6-diamino-2-phenyl indole (DAPI, 1 µg/mL) solution for 10 min. Finally, the cellular uptake of cells in each well was observed with the confocal laser scanning microscopy (CLSM).

#### 2.8. Cellular singlet oxygen detection

The level of intracellular singlet oxygen was detected by 2,7-dichlorofluorescein diacetate (DCFH-DA), which can be oxidized to dichlorofluorescein (DCF) in the presence of singlet oxygen [30]. HeLa cells were firstly cultured for 24 h in a 48-well plate. Then the original medium was replaced with a fresh medium containing IR6, IR7, and IR8 (40 µg/mL) and incubated for 4 h. After that, HeLa cells were washed with PBS for 3 times and incubated with DCFH-DA for 20 min. Finally, the cells were irradiated with an 808 nm laser (1.0 W/cm<sup>2</sup>), and the fluorescence images of the cells were observed using a fluorescence microscope.

#### 2.9. Cell culture and cytotoxicity test

The cell cytotoxicity of dye was evaluated by the methyl thiazolyltetrazolium (MTT) assay [31]. HeLa cells were cultured in Dulbecco's modified Eagle's medium (DMEM, Thermal Fisher Scientific). HeLa cells in 96-well plates (100 µL,  $1 \times 10^5$  cells/mL) were incubated for 24 h under hypoxic condition (37 °C, 5% CO<sub>2</sub>). Then, IR6, IR7, and IR8 with different concentrations (0, 10, 20, 40, 80, 100 µg/mL) dissolved in DMEM were added to the wells and incubated for 24 h. After that, MTT solution (100 µL, 0.5 mg/mL) was added to each well and the plate was incubated for an additional 4 h. Each well was then washed with phosphate-buffered saline (PBS) and added dimethyl sulfoxide (DMSO, 100 µL). After the formazan was fully dissolved, the absorbance of each

sample at 490 nm was recorded using a plate reader.

### 2.10. PTT and PDT synergistic therapy *in vitro*

HeLa cells were seeded in a 96-well plate ( $1 \times 10^5$  cells/mL). After 24 h of incubation, the medium was replaced with fresh medium containing dyes (IR6, IR7, and IR8) with different concentrations (0, 20, 40, 80, 100  $\mu\text{g/mL}$ ) and incubated for 12 h. Then, each well was irradiated using a NIR laser (808 nm,  $1.0 \text{ W/cm}^2$ ) for 5 min. After that, the cells were washed with PBS. Finally, the MTT solution (100  $\mu\text{L}$ , 0.5 mg/mL) was added to each well and cultured for 4 h to evaluate the photothermal and photodynamic effects *in vitro*.

## 3. Results and discussion

### 3.1. Synthesis and characterization

Halogenated cyanine dyes (IR6, IR7, and IR8) were synthesized by introducing Cl, Br, or I atoms into position 5 of the indole skeleton, respectively. The general synthesis procedures for IR6, IR7, and IR8 are shown in Fig. S1. Besides, compound IR7 and IR8 were prepared according to the reported method [25,26]. The structures of all dyes were confirmed by  $^1\text{H}$  NMR,  $^{13}\text{C}$  NMR, ESI-MS, and MALDI-TOF-MS analysis.

### 3.2. Optical properties

The absorption and fluorescence spectra of IR6, IR7, and IR8 were obtained. As shown in Fig. 2a and b, the maximal absorption peaks of IR6, IR7, and IR8 were located at 790, 793, and 796 nm in methanol. However, the emission peaks of IR6, IR7, and IR8 were at 836, 837, and 844 nm, respectively. We can observe that the introduction of heavy atoms will make the absorption and emission wavelength of dyes redshift, which was positively correlated with the increase of the atomic number of the halogen atom.

### 3.3. Singlet oxygen generation *in vitro*

To evaluate the photodynamic properties of IR6, IR7, and IR8, DPBF was used to detect the singlet oxygen generation of dyes. As a singlet oxygen detector, DPBF can occur degradation when it reacted with singlet oxygen. Therefore, the change in the absorbance of DPBF can be used to observe the generation of singlet oxygen. The change in absorbance of DPBF under laser irradiation in water and DMF was negligible, indicating that no singlet oxygen was produced (Fig. S14a). The absorbance of DPBF with IR6, IR7, and IR8 displayed a significant drop at 418 nm under irradiation of NIR light, confirming their ability to generate singlet oxygen (Figs. S14b, c, and d). The singlet oxygen generation of IR8 was higher than that of IR6 and IR7 (The absorbance of DPBF was reduced by 78.3%, 63.4%, and 32.6%, respectively), indicating that the iodine atom had the greatest impact on generating singlet oxygen. Besides, it was worth noting that IR6 has a better singlet oxygen generation ability than IR7. The reason may be that cyanine dye with bromine atom was more likely to form J-aggregates in aqueous systems, resulting in a decrease in the lifetime of the triplet excited state, decreasing ability for singlet oxygen generation [32–34].

Therefore, we measured the absorption spectra of IR6, IR7, and IR8 in aqueous solutions. As shown in Fig. 2c, IR6 only had its monomer absorption peak at 788 nm. However, IR7 not only had the monomer absorption peak in 800 nm but also showed the absorption peak of the J-aggregates at 926 nm. This proved that IR7 formed J-aggregates in the aqueous solution, causing the aggregation-caused quenching (ACQ) effect and reducing the generation of singlet oxygen. As shown in Fig. 2d, we only found that the monomer absorption peaks of IR6, IR7, and IR8 were located at 800, 802, and 806 nm in DMF. Meanwhile, as shown in Fig. 3b, it was observed that the singlet oxygen generation of IR6, IR7, and IR8 showed a positive correlation with the increased relative atomic

mass of halogen atoms, which further confirmed the previous analysis.

### 3.4. Photothermal property

The photothermal effects of IR6, IR7, and IR8 were evaluated. As shown in Fig. 4a, the temperature of IR6, IR7, and IR8 solutions (40  $\mu\text{g/mL}$ ) increased 27.3  $^\circ\text{C}$ , 37.1  $^\circ\text{C}$ , and 42.7  $^\circ\text{C}$ . This result indicated the excellent photothermal property of IR6, IR7, and IR8. Therefore, it was concluded that the photothermal effects showed a positive correlation with the increased relative atomic mass of halogen atoms. The photothermal conversion efficiency ( $\eta$ ) of IR6, IR7, and IR8 solutions was calculated as 42.3%, 43.4%, 46.6%, which further confirmed the experiment results.

Then we evaluated the effect of IR6, IR7, and IR8 concentration on temperature rise (Figs. S16b, c, and d). IR6, IR7, and IR8 all displayed different degrees of temperature rise with increasing concentration.

In order to investigate the photothermal stability of dyes, IR6, IR7, and IR8 were irradiated by the multiple laser with recording the irradiated temperature changes. However, the maximum temperatures of IR6, IR7, and IR8 showed varying decreased degrees during four cycles. The differences between the first and last cycles of the maximum temperature of IR6, IR7, and IR8 were 17.3  $^\circ\text{C}$ , 9.5  $^\circ\text{C}$ , and 8.7  $^\circ\text{C}$ , respectively. The experiment results indicated that IR6, IR7, and IR8 had not a good photostability, which were positively related to the increased relative atomic mass of halogen atoms.

### 3.5. Cellular uptake

The uptakes of HeLa cells to IR6, IR7, and IR8 were investigated using the confocal laser scanning microscopy (CLSM). As shown in Fig. 5, after having incubated with IR6 for 0.5 h, 2 h, and 6 h, the fluorescence brightness (FB) obviously increased in the red fluorescence channel. This means cellular uptake of IR6 gradually increased over time. Similarly, as shown in Figs. S17 and S18, HeLa cells incubated with IR7, and IR8 also showed increased cellular uptake to dyes over time.

### 3.6. Cellular singlet oxygen detection

The generation of singlet oxygen in cells under the laser irradiation was detected using DCFH-DA (2,7-dichloro-dihydro-fluorescein diacetate). DCFH-DA would be hydrolyzed into non-fluorescent DCFH (2,7-dichlorofluorescein) in the cell, which was oxidized by singlet oxygen into green fluorescent DCF (dichlorofluorescein). Fig. 6 showed the cells incubated with IR6, IR7, and IR8 possessed negligible green fluorescence without laser irradiation. In contrast, the cells with laser irradiation showed bright green fluorescence. These results showed that IR6, IR7, and IR8 could produce singlet oxygen effectively in cells and had great potential for PDT.

### 3.7. Cell cytotoxicity *in vitro*

MTT assay was used to reveal the cell cytotoxicity of IR6, IR7, and IR8. MTT (3-(4,5-dimethyl-2-thiazolyl)-2,5-diphenyl-2-tetrazolium bromide) would be reduced to formazan (purple solid could dissolve in DMSO) by succinate dehydrogenase in living cells [31]. As shown in Fig. 7, different concentrations of IR6, IR7, and IR8 were added to HeLa cells, MTT value was measured after cell incubation for 24 h. Even with concentration at 100  $\mu\text{g/mL}$ , the cell viability of IR6, IR7, and IR8 were still over 80%, indicating the low cytotoxicity of IR6, IR7, and IR8.

### 3.8. PTT and PDT synergistic therapy *in vitro*

The phototherapy effects of IR6, IR7, and IR8 were investigated against HeLa cells using standard MTT assay. As shown in Fig. 8, different concentrations of IR6, IR7, and IR8 were added to HeLa cells, and the cells were irradiated with NIR irradiation for 5 min. The MTT

value was measured after 24 h. IR8 showed a more effective cytostatic effect (half-maximal inhibitory concentration,  $IC_{50} = 16.2 \mu\text{g/mL}$ ) than IR6 and IR7 in agreement with the photothermal and photodynamic experiment results in solution-based. However, IR6 displayed better phototherapy effects than IR7, possibly due to IR7 can effectively generate higher singlet oxygen.

Through comparison of IR6, IR7, and IR8 in solution-based and cell-based experiments, we came to the conclusion that IR8 had a low dark toxicity and high phototherapy effect among all halogenated cyanine dyes. IR7 presented suboptimal light toxicity than IR6. Halogenated cyanine dyes did not strictly behave a more effective phototherapy effect as the number of halogenated atoms increases.

#### 4. Conclusion

In summary, we synthesized three halogenated cyanine dyes through general procedures and evaluated the influence of heavy atoms on the photothermal and photodynamic performance of cyanine. The introduction of heavy atoms would cause a redshift in the absorption and emission wavelength of the cyanine. Meanwhile, the effect of heavy atoms on the singlet oxygen generation capacity, photothermal conversion efficiency, and photothermal stability was positively correlated with the increase of the atomic number of the halogen atom. IR6, IR7, and IR8 all exhibited low dark toxicity. Finally, cyanine IR8 undoubtedly exhibited the best reactive oxygen generation capacity, photothermal conversion rate, and therapeutic efficiency over IR6, and IR7. The influence of heavy atoms on cyanine dyes of this work can provide guidance to design other phototherapy agents with high photodynamic and photothermal effects in the NIR region.

#### Declaration of competing interest

The authors declare that they have no known competing financial interests or personal relationships that could have appeared to influence the work reported in this paper.

#### Acknowledgements

This work was financially supported by the National Natural Science Foundation of China (NSFC, Nos. 21676187).

#### Appendix A. Supplementary data

Supplementary data to this article can be found online at <https://doi.org/10.1016/j.dyepig.2021.109327>.

#### Author statement

Hao Liu: Conceptualization, Methodology, Software, Validation, Investigation, Formal analysis, Resources, Data curation, Writing – original draft, Writing – review & editing. Juanjuan Yin: Software, Resources. Enyun Xing: Validation. Yingying Du: Validation, Formal analysis. Yu Su: Validation. Yaqing Feng: Conceptualization, Writing – review & editing. Writing Review and Editing, Visualization, Supervision, Project administration, Funding acquisition. Shuxian Meng: Conceptualization, Methodology, Writing – review & editing. Writing Review and Editing, Visualization, Supervision, Project administration, Funding acquisition

#### References

- Li Z, Tan S, Li S, Shen Q, Wang K. Cancer drug delivery in the nano era: an overview and perspectives (Review) *Oncol Rep* 2017;38(2):611–24. <https://doi.org/10.3892/or.2017.5718>.
- Liu Y, Bhattarai P, Dai Z, Chen X. Photothermal therapy and photoacoustic imaging via nanotheranostics in fighting cancer. *Chem Soc Rev* 2019;48(7):2053–108. <https://doi.org/10.1039/c8cs00618k>.
- Wang X, Zhang J, Wang Y, Wang C, Xiao J, Zhang Q, et al. Multi-responsive photothermal-chemotherapy with drug-loaded melanin-like nanoparticles for synergistic tumor ablation. *Biomaterials* 2016;81:114–24. <https://doi.org/10.1016/j.biomaterials.2015.11.037>.
- Zou Q, Abbas M, Zhao L, Li S, Shen G, Yan X. Biological photothermal nanodots based on self-assembly of peptide porphyrin conjugates for antitumor therapy. *J Am Chem Soc* 2017;139(5):1921–7. <https://doi.org/10.1021/jacs.6b11382>.
- Zhang P, Hu C, Ran W, Meng J, Yin Q, Li Y. Recent progress in light-triggered nanotheranostics for cancer treatment. *Theranostics* 2016;6(7):948–68. <https://doi.org/10.7150/thno.15217>.
- Zhu A, Miao K, Deng Y, Ke H, He H, Yang T, et al. Dually pH/reduction-responsive vesicles for ultrahigh-contrast fluorescence imaging and thermo-chemotherapy-synergized tumor ablation. *ACS Nano* 2015;9(8):7874–85. <https://doi.org/10.1021/acsnano.5b02843>.
- He H, Zhou J, Liu Y, Liu S, Xie Z, Yu M, et al. Near-infrared-light-induced morphology transition of poly(ether amine) nanoparticles for supersensitive drug release. *ACS Appl Mater Interfaces* 2018;10(8):7413–21. <https://doi.org/10.1021/acsaami.8b00194>.
- Xing Y, Ding T, Wang Z, Wang L, Guan H, Tang J, et al. Temporally controlled photothermal/photodynamic and combined therapy for overcoming multidrug resistance of cancer by polydopamine nanoclustered micelles. *ACS Appl Mater Interfaces* 2019;11(15):13945–53. <https://doi.org/10.1021/acsaami.9b00472>.
- Pais-Silva C, de Melo-Diogo D, Correia LJ. IR780-loaded TPGS-TOS micelles for breast cancer photodynamic therapy. *Eur J Pharm Biopharm* 2017;113:108–17. <https://doi.org/10.1016/j.ejpb.2017.01.002>.
- Thomas AP, Palanikumar L, Jeena MT, Kim K, Ryu J-H. Cancer-mitochondria-targeted photodynamic therapy with supramolecular assembly of HA and a water soluble NIR cyanine dye. *Chem Sci* 2017;8(12):8351–6. <https://doi.org/10.1039/c7sc03169f>.
- Ma S, Zhou J, Zhang Y, Yang B, He Y, Tian C, et al. An oxygen self-sufficient fluorinated nanoplatform for relieved tumor hypoxia and enhanced photodynamic therapy of cancers. *ACS Appl Mater Interfaces* 2019;11(8):7731–42. <https://doi.org/10.1021/acsaami.8b19840>.
- Ma Y, Zhang M, Li P, Han Z, Wu L, Li T, et al. Multifunctional small molecule fluorophore for long-duration tumor-targeted monitoring and dual modal phototherapy. *Part Part Syst Char* 2017;34(7):1700076. <https://doi.org/10.1002/ppsc.201700076>.
- Cao J, Chi J, Xia J, Zhang Y, Han S, Sun Y. Iodinated cyanine dyes for fast near-infrared-guided deep tissue synergistic phototherapy. *ACS Appl Mater Interfaces* 2019;11(29):25720–9. <https://doi.org/10.1021/acsaami.9b07694>.
- Zhang RR, Schroeder AB, Grudzinski JJ, Rosenthal EL, Warram JM, Pinchuk AN, et al. Beyond the margins: real-time detection of cancer using targeted fluorophores. *Nat Rev Clin Oncol* 2017;14(6):347–64. <https://doi.org/10.1038/nrclinonc.2016.212>.
- Cardillo JA, Jorge R, Costa RA, Nunes SMT, Lavinsky D, Kuppermann BD, et al. Experimental selective choriocapillaris photothrombosis using a modified indocyanine green formulation. *Br J Ophthalmol* 2008;92(2):276–80. <https://doi.org/10.1136/bjo.2007.129395>.
- Yang P, Cao Y, Zhang L, Yao X, Yang W, Men Y, et al. Metal-organic framework nanoparticles with near-infrared dye for multimodal imaging and guided phototherapy. *ACS Appl Mater Interfaces* 2019;11(12):11209–19.
- Shao N, Qi Y, Lu H, He D, Li B, Huang Y. Photostability highly improved nanoparticles based on IR-780 and negative charged copolymer for enhanced photothermal therapy. *ACS Biomater Sci Eng* 2018;5(2):795–804. <https://doi.org/10.1021/acsbomaterials.8b01558>.
- Tan X, Luo S, Wang D, Su Y, Cheng T, Shi C. A NIR heptamethine dye with intrinsic cancer targeting, imaging and photosensitizing properties. *Biomaterials* 2012;33(7):2230–9. <https://doi.org/10.1016/j.biomaterials.2011.11.081>.
- Gao G, Jiang YW, Sun W, Guo Y, Jia HR, Yu XW, et al. Molecular targeting-mediated mild-temperature photothermal therapy with a smart albumin-based nanodrug. *Small* 2019;15(33):e1900501. <https://doi.org/10.1002/sml.201900501>.
- Lin W, Li Y, Zhang W, Liu S, Xie Z, Jing X. Near-infrared polymeric nanoparticles with high content of cyanine for bimodal imaging and photothermal therapy. *ACS Appl Mater Interfaces* 2016;8(37):24426–32. <https://doi.org/10.1021/acsaami.6b07103>.
- Luo S, Yang Z, Tan X, Wang Y, Zeng Y, Wang Y, et al. Multifunctional photosensitizer grafted on polyethylene glycol and polyethylenimine dual-functionalized nanographene oxide for cancer-targeted near-infrared imaging and synergistic phototherapy. *ACS Appl Mater Interfaces* 2016;8(27):17176–86. <https://doi.org/10.1021/acsaami.6b05383>.
- Luo S, Tan X, Qi Q, Guo Q, Ran X, Zhang L, et al. A multifunctional heptamethine near-infrared dye for cancer theranosis. *Biomaterials* 2013;34(9):2244–51. <https://doi.org/10.1016/j.biomaterials.2012.11.057>.
- Atchison J, Kamila S, Nesbitt H, Logan KA, Nicholas DM, Fowley C, et al. Iodinated cyanine dyes: a new class of sensitizers for use in NIR activated photodynamic therapy (PDT). *Chem Commun* 2017;53(12):2009–12. <https://doi.org/10.1039/c6cc09624g>.
- Dean-Ben XL, Gottschalk S, Mc Larny B, Shoham S, Razansky D. Advanced optoacoustic methods for multiscale imaging of in vivo dynamics. *Chem Soc Rev* 2017;46(8):2158–98. <https://doi.org/10.1039/c6cs00765a>.
- Jing T, Fu L, Liu L, Yan L. A reduction-responsive polypeptide nanogel encapsulating NIR photosensitizer for imaging guided photodynamic therapy. *Polym Chem* 2016;7(4):951–7. <https://doi.org/10.1039/c5py01629k>.

- [26] Usama SM, Thavornpradit S, Burgess K. Optimized heptamethine cyanines for photodynamic therapy. *ACS Applied Bio Materials* 2018;1(4):1195–205. <https://doi.org/10.1021/acsabm.8b00414>.
- [27] Pan G-Y, Jia H-R, Zhu Y-X, Wang R-H, Wu F-G, Chen Z. Dual channel activatable cyanine dye for mitochondrial imaging and mitochondria-targeted cancer theranostics. *ACS Biomater Sci Eng* 2017;3(12):3596–606. <https://doi.org/10.1021/acsbiomaterials.7b00480>.
- [28] Ren W, Yan Y, Zeng L, Shi Z, Gong A, Schaaf P, et al. A near infrared light triggered hydrogenated black TiO<sub>2</sub> for cancer photothermal therapy. *Advanced Healthcare Materials* 2015;4(10):1526–36. <https://doi.org/10.1002/adhm.201500273>.
- [29] Liu Y, Ai K, Liu J, Deng M, He Y, Lu L. Dopamine-Melanin colloidal nanospheres: an efficient near-infrared photothermal therapeutic agent for in vivo cancer therapy. *Adv Mater* 2013;25(9):1353–9. <https://doi.org/10.1002/adma.201204683>.
- [30] Li N, Xu F, Cheng J, Zhang Y, Huang G, Zhu J, et al. Perfluorocarbon nanocapsules improve hypoxic microenvironment for the tumor ultrasound diagnosis and photodynamic therapy. *J Biomed Nanotechnol* 2018;14(12):2162–71. <https://doi.org/10.1166/jbn.2018.2656>.
- [31] Su Y, Wang N, Liu B, Du Y, Li R, Meng Y, et al. A phototheranostic nanoparticle for cancer therapy fabricated by BODIPY and graphene to realize photo-chemo synergistic therapy and fluorescence/photothermal imaging. *Dyes Pigments* 2020; 177:108262. <https://doi.org/10.1016/j.dyepig.2020.108262>.
- [32] Alex S, Basheer MC, Arun KT, Ramaiah D, Das S. Aggregation properties of heavy atom substituted squaraine Dyes: evidence for the formation of J-type dimer aggregates in aprotic solvents. *J Phys Chem* 2007;111(17):3226–30. <https://doi.org/10.1021/jp068492a>.
- [33] Würthner F, Kaiser TE, Saha-Möller CR. J-aggregates: from serendipitous discovery to supramolecular engineering of functional dye materials. *Angew Chem Int Ed* 2011;50(15):3376–410. <https://doi.org/10.1002/anie.201002307>.
- [34] Zhang YH, Li X, Huang L, Kim HS, An J, Lan M, et al. AIE based GSH activatable photosensitizer for imaging-guided photodynamic therapy. *Chem Commun* 2020; 56(71):10317–20. <https://doi.org/10.1039/d0cc02045a>.